Geomechanics and Engineering, *Vol. 23, No. 4 (2020) 313-325*
DOI: https://doi.org/10.12989/gae.2020.23.4.313

The expanded LE Morgenstern-Price method for slope stability analysis based on a force-displacement coupled mode

Dong-ping Deng*, Kuan Lu[a], Sha-sha Wen[b] and Liang Li[c]

School of Civil Engineering, Central South University, Changsha 410075, China

(Received August 3, 2020, Revised October 17, 2020, Accepted October 26, 2020)

Abstract. Slope displacement and factor of safety (FOS) of a slope are two aspects that reflect the stability of a slope. However, the traditional limit equilibrium (LE) methods only give the result of the slope FOS and cannot be used to solve for the slope displacement. Therefore, developing a LE method to obtain the results of the slope FOS and slope displacement has significance for engineering applications. Based on a force-displacement coupled mode, this work expands the LE Morgenstern-Price (M-P) method. Except for the mechanical equilibrium conditions of a sliding body adopted in the traditional M-P method, the present method introduces a nonlinear model of the shear stress and shear displacement. Moreover, the energy equation satisfied by a sliding body under a small slope displacement is also applied. Therefore, the double solutions of the slope FOS and horizontal slope displacement are established. Furthermore, the flow chart for the expanded LE M-P method is given. By comparisons and analyses of slope examples, the present method has close results with previous research and numerical simulation methods, thus verifying the feasibility of the present method. Thereafter, from the parametric analysis, the following conclusions are obtained: (1) the shear displacement parameters of the soil affect the horizontal slope displacement but have little effect on the slope FOS; and (2) the curves of the horizontal slope displacement vs. the minimum slope FOS could be fitted by a hyperbolic model, which would be beneficial to obtain the horizontal slope displacement for the slope in the critical state.

Keywords: slope stability; limit equilibrium; Morgenstern-Price method; force-displacement coupled mode; factor of safety; horizontal slope displacement

1. Introduction

The limit equilibrium (LE) method is commonly used to analyze slope stability as the recommended method in the slope design specification (Vanneschi *et al.* 2018; Deng *et al.* 2019; Guo *et al.* 2020). At present, more than a dozen LE methods have been proposed, and most of them are deduced on the basis of the slice method. The concept of the slice method was first proposed by Petterson (the Swedish scholar) in 1916 (Mohtarami *et al.* 2014), and it can be used to solve the statically indeterminate problem of slope stability when the slip surface is curved. Thereafter, based on the slice approach, the LE methods for slope stability were constantly developed and improved by predecessors with different assumptions on the interslice forces. It should be noted that the early LE methods such as the Bishop method (Bishop 1955) were only suitable for slope stability analysis with a circular slip surface and the later improved methods could be used for other shaped slip surfaces.

Among the many established LE method, the Morgenstern-Price (M-P) method (Morgenstern and Price 1965) is a famous rigorous method that satisfies all the mechanical equilibrium conditions of the sliding body. The assumption of a reasonably nonlinear relationship between the interslice shear force and normal force was adopted by the M-P method. Moreover, the M-P method modifies the interslice forces with a smooth curve function to ensure good convergence when the slope factor of safety (FOS) is solved iteratively. Due to the above advantages of the M-P method, Chen and Morgenstern (1983) improved the original M-P method and proposed an analytical solution of the M-P method to solve for the slope FOS; Zhu *et al.* (2005) established a concise calculation formula for the M-P method in nondifferential form; Sun *et al.* (2016) developed a global procedure for the stability analysis of slopes by combining the numerical stability of the global analysis method and the flexibility of the M-P method; and Wang *et al.* (2019) carried out on the probabilistic risk assessment of slope failure by combining the M-P method. So far, the latest research results using the M-P method to solve for slope stability under complex conditions are still emerging (Bai *et al.* 2014, Mandal *et al.* 2019, Himanshu *et al.* 2020, Siacara *et al.* 2020).

Although the M-P method is nearly perfect in the theoretical evaluation of slope stability, landslides have still been continuously reported in recent years. Thus, slope displacement monitoring has become a hot topic. However, traditional LE methods only give the result of the FOS of a slope and cannot yield slope displacement (Yamaguchi *et al.* 2018). Therefore, developing a new LE method to obtain the double solutions of the slope FOS and slope displacement would be beneficial to the application of slope

*Corresponding author, Associate Professor, Ph.D.
E-mail: dengdp851112@126.com
[a]Master Student
[b]Master Student
[c]Professor, Ph.D.

ISSN: 2005-307X (Print), 2092-6219 (Online)

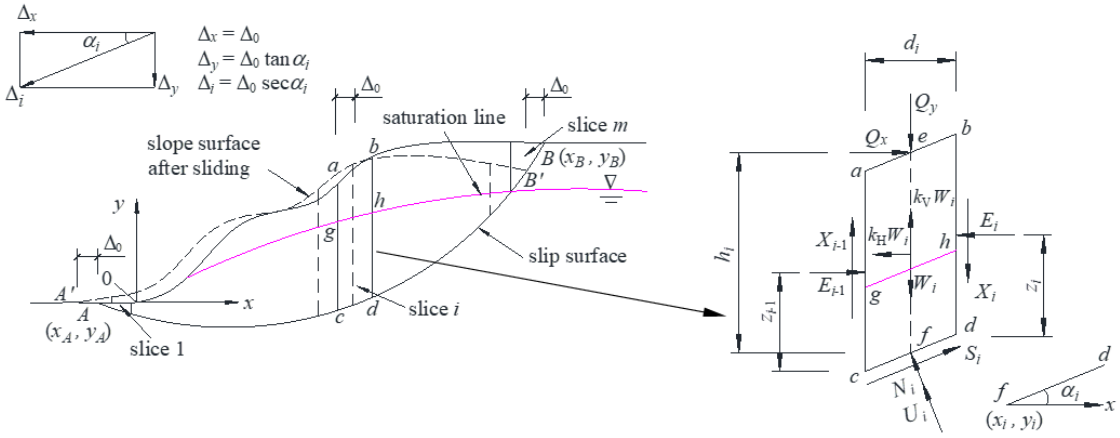

Fig. 1 Calculation model of LE analysis for slope stability based on force-displacement coupled mode

displacement monitoring data and to reflect slope security under the corresponding slope displacement. Further, it could provide an early warning for the occurrence of landslides (Ghanbari *et al.* 2013).

With the development of computing technology and the innovation of numerical simulation methods, solving for the slope displacement has become easy, and it can be performed by the finite element method (FEM) (Tran *et al.* 2019), the finite difference method (FDM) (Gong and Tang 2016), and so on. Nevertheless, the accuracy of the numerical simulation results depends on the detailed stress-strain constitutive parameters of all geotechnical materials. Some of these parameters are not easily obtained by in situ testing, thus limiting the application of the numerical simulation methods. McCombie (2009) developed a theoretical method to analyze the slope displacement based upon multiple wedges. This theoretical method works from simple assumptions about the kinematics of movement, increasing displacements and hence resisting forces iteratively until force equilibrium is attained. Since it only applies to the sliding body with multiple wedges, McCombie's method is still not convenient for calculating the displacement of slope with other shaped sliding body. Huang (2013) proposed an innovative calculation method for slope displacement by introducing a constitutive model of the shear stress and shear displacement on the slip surface into the Janbu method. Subsequently, Huang (2014) analyzed the finite displacement of a reinforced slope with his own method. Thereafter, Cheng and Zhou (2015) and Zhou *et al.* (2019) developed the three-dimensional (3D) displacement-based rigorous LE method on the basis of Huang's method. Huang and follow-up researchers have made important contributions to solve for the slope displacement using the LE methods, and their studies verified that it was feasible to calculate the slope displacement by applying the relationship of the shear stress vs. the shear displacement. However, Huang's method still has some deficiencies. For example, since no other condition (such as the energy equation) has been introduced, Huang's method solves for the slope displacement (i.e., the displacement on the slip surface) instead of the slope FOS by the mechanical equilibrium conditions, as done in the traditional LE methods. In other words, double solutions of the slope displacement and slope FOS cannot be obtained by Huang's method to reveal the relationship between the slope stability and slope displacement. Moreover, the formula of the slope displacement in Huang's method is an implicit one, which reduces the calculation efficiency. In addition, Huang's method inherits the deficiency of the traditional Janbu method, i.e., the calculation convergence becomes worse with the increase in the number of divided slices.

Here, with the assumption that the slope sliding body is a rigid body, a calculation model of the horizontal slope displacement is constructed on the basis of the displacement compatibility for a slope under small slope displacement. The horizontal slope displacement is also expressed as the horizontal displacement on the slope surface so that the displacement monitoring data on the slope surface can be applied to the present model. Thereafter, with the introduction of the constitutive model of the shear stress and shear displacement on the slip surface, the LE M-P method is expanded to analyze slope stability based on a force-displacement coupled mode. Then, the mechanical equilibrium conditions and energy equation satisfied by the slope sliding body are used to derive the formula of the slope FOS and horizontal slope displacement, respectively. Thus, double solutions of the slope FOS and horizontal slope displacement are obtained. In the present method, the formula of horizontal slope displacement is explicit to improve the calculation speed. Furthermore, the relationship of the horizontal slope displacement vs. the slope FOS is revealed from parametric analysis.

2. Expanded LE M-P method based on the force-displacement coupled mode

2.1 Solution of slope FOS in the expanded LE M-P method

Fig. 1 shows the calculation model of the LE analysis for slope stability based on the force-displacement coupled mode. In Fig. 1, the *xy*-axis coordinate system is established with the slope toe as the origin. The lower and upper sliding points of the slip surface are represented as *A* and *B*,

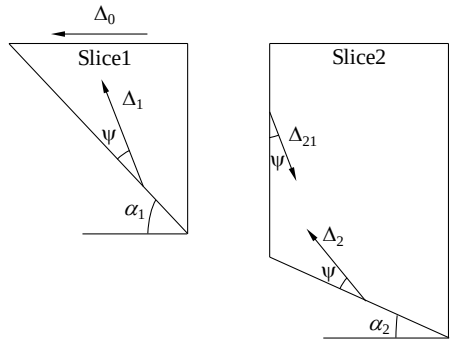

(a) Vectors of shear displacement

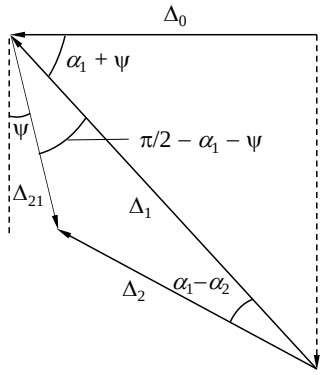

(b) Displacement diagram

Fig. 2 Displacement compatibility of adjacent slices

respectively. To solve for the slope stability of a curved slip surface, the traditional LE methods use the slice method and divide the sliding body into *m* vertical slices from point *A* to point *B*. For the *i*-th slice under the shear force (or the shear stress), shear displacement Δ_i (i = 1, 2, …, m) exists along the slip surface. According to the displacement diagram (Huang 2013) that satisfies the displacement compatibility (Atkinson 1981) shown in Figs. 2(a) and 2(b), the shear displacement of slice 2 has a relationship with slice 1 as follows:

$$\Delta_2 = \Delta_1 \frac{\cos(\alpha_1 + 2\psi)}{\cos(2\psi + \alpha_2)} \tag{1}$$

where ψ is dilatancy angle and $\Delta_1 = \Delta_0 / \cos(\alpha_1 + \psi)$, Δ_0 is the horizontal slope displacement at the slope toe.

Eq. (1) also represents the recurrence relation of the shear displacements along the slip surface between the two adjacent slices Thus, the shear displacement of slice *i* can be related to the horizontal slope displacement (Δ_0) at the slope toe using:

$$\Delta_i = \frac{\Delta_0}{\cos(\alpha_1 + \psi)} \frac{\cos(\alpha_1 + 2\psi)}{\cos(2\psi + \alpha_i)} \tag{2}$$

where α_i (i = 1, 2, …, m) is the horizontal angle of the tangent to the slip surface in slice *i*, and it is positive in the counterclockwise direction and negative in the clockwise direction.

When $\psi = 0$ in Eq. (2), meaning that the dilatancy effect of the soil is not considered in the slope stability analysis, Eq. (2) can be simplified into:

$$\Delta_i = \Delta_0 / \cos\alpha_i \tag{3}$$

Eq. (3) demonstrates that slice *i* has the same horizontal displacement as the horizontal slope displacement (Δ_0) at the slope toe and that Δ_0 is also called the horizontal slope displacement. In other words, the slope would horizontally slide as a whole with the assumption that the slope sliding body is a rigid body when the dilatancy effect of the soil is not considered. In fact, for the slope in a stable state (i.e., the minimum slope FOS is greater than 1.000), the slope displacement is very small compared to the size of the sliding body. Therefore, it is feasible to regard slope sliding as the whole movement along the slip surface or ground for the slope sliding body. Moreover, shear dilatancy is usually an important characteristic of particulate materials, such as sand and coarse-grained soil. For clayey soils (especially the normally consolidated clayey soil), the shear dilatancy of the soil is not very obvious when the slope slides. Thus, Eq. (3) is adopted as the displacement compatibility conditions of the rigid sliding body to analyze the stability of the clayey soil slope with the force-displacement coupled mode. Without considering the shear dilatancy of the soil, it is also easy to calculate the work done by the gravity and external force on slice *i* to establish the energy equation of the sliding body.

According to the above analysis, the slope surface after sliding under the small horizontal slope displacement could be obtained. That is, the average horizontal displacement (i.e., Δ_0 shown in Fig. 1) of the slope surface would be obtained theoretically as done in the slope stability analysis for calculating the general slope FOS. In practical engineering, the potential real slip surface of the slope is unknown, although the approximate potential slip surface of the slope could be obtained by theoretical methods. Therefore, the displacement of the slip surface is difficult to obtain by field monitoring. However, the displacement of the slope surface is easily obtained by arranging the monitoring points on the slope surface. Thus, the present method could be combined with the displacement monitoring data on the slope surface to study the relationship between the slope stability and the slope displacement.

After the model of the slope displacement is analyzed, the force analysis on the sliding body needs to be carried out. Then, with the introduction of the constitutive relationship between the shear stress and shear displacement, the purpose of analyzing the slope stability based on the force-displacement mode would be achieved. For vertical slice *i* (i.e., slice *abcd* in Fig. 1), the width d_i is selected to analyze the forces acting on it. In slice *i*, part *cdgh* is below the groundwater table, part *abgh* is above the groundwater table, *f* is the midpoint of the slip surface *cd* with the coordinate of (x_i, y_i), *e* is the intersection point between the vertical line passing through point *f* and the slope surface, h_i is the height of the vertical centerline *ef*, and $z_{i\text{-}1}$ and z_i are the vertical distances between the horizontal interslice forces (i.e., $E_{i\text{-}1}$ and E_i) and the base of the slice, respectively. Under normal conditions, the following forces act on slice *i*: (1) the gravity W_i; (2) the horizontal seismic force $k_H W_i$ and the vertical seismic force

$k_V W_i$; (3) the external forces Q_x (horizontal direction) and Q_y (vertical direction) on the slope surface; (4) the shear forces X_i and X_{i-1} on the two sides of the vertical slice; (5) the normal forces E_i and E_{i-1} on the two sides of the vertical slice; (6) the normal force N_i on the slip surface; (7) the shear force S_i on the slip surface; and (8) the pore water force U_i on the slip surface. Among the above parameters, k_H and k_V are the horizontal and vertical seismic action coefficients, respectively.

As shown in Fig. 1, the force equilibrium conditions for all the forces along the normal and tangential directions to the slip surface in slice i are given as follows:

$$N_i = (X_i - X_{i-1})\cos\alpha_i - (E_i - E_{i-1})\sin\alpha_i + (W_i - k_H W_i + Q_y)\cos\alpha_i - (k_V W_i - Q_x)\sin\alpha_i - U_i \quad (4)$$

$$S_i = (X_i - X_{i-1})\sin\alpha_i + (E_i - E_{i-1})\cos\alpha_i + (W_i - k_V W_i + Q_y)\sin\alpha_i + (k_H W_i - Q_x)\cos\alpha_i \quad (5)$$

where $U_i = r_u W_i$ and r_u is the pore-water pressure coefficient.

According to the assumption of interslice forces in the M-P method (Morgenstern and Price 1965), the relationship between the interslice shear force (X_i) and the normal force (E_i) can be calculated as follows:

$$X_i = \lambda f_i E_i \quad (6)$$

where λ is the calculation parameter, f_i is the correction function of the interslice forces, which is usually a half-sine function, and $f_i = \sin[(x_i - x_A)\pi / (x_B - x_A)]$.

For the constitutive relationship between the shear stress and shear displacement, Huang (2013) established their relationship by applying the nonlinear curve of the shear stress vs. the shear strain in the soil from the research of Kondner (1963) and Duncan and Chang (1970). The curve of the shear stress vs. the shear strain (or the shear stress vs. the shear displacement) would be approximated by a hyperbola with a high degree of accuracy (Zhou *et al.* 2019). In addition, the shear displacement of slip surface in the slope is equal to its shear strain times the corresponding thickness of the shear band. Thus, the relationship between the shear stress and shear displacement on the slip surface of slice i is given as follows:

$$\tau_i = \frac{\Delta_i}{a_i' + b'\Delta_i} \quad (7)$$

where τ_i is the shear stress on the base of slice i, $\tau_i = S_i / (d_i \sec\alpha_i)$, $a' = 1 / k_{initial}$, $b' = R_f / \tau_f$, $k_{initial}$ is the initial value of the shear spring constant to describe the potential relationship between shear displacement and shear stress with introduction of the thickness of the shear band, R_f is the failure ratio related to the type of soil with a range of 0.7 ~ 0.9 (Duncan and Chang 1970), and τ_f is the shear strength. According to the relationship between the shear stress and shear displacement on the slip surface, expressed by Eq. (7), it could be viewed as a Winkler-type series of non-linear, tangential "springs" distributed along the slip surface. It should be noted that the interactions between the springs could not be considered strictly in the LE methods because of the assumption of the rigid body for the sliding body. However, the interactions between springs are still involved by introducing the inter-slice forces (see Fig. 1) and satisfying the displacement compatible condition between slices (see Eq. (2)).

Substituting Eq. (3) into Eq. (7), and converting Eq. (7) yields the relationship between the shear stress (τ_i) on the slip surface of slice i and the slope horizontal displacement (Δ_0) as follows:

$$\tau_i = \frac{\Delta_0}{a_i \cos\alpha_i + b_i \Delta_0}\tau_f \quad (8)$$

where $a_i = \tau_f / k_{\text{initial}}$ and $b_i = R_f$.

Related to the parameters a_i' (Eq. (7)) and a_i (Eq. (8)), the initial modulus k_{initial} is the exponential function of the normal pressure (σ_i) on the slip surface (Duncan and Chang 1970). For slice i, k_{initial} is computed as follows:

$$k_{\text{initial}} = K \cdot P_a \cdot \left(\frac{\sigma_i}{P_a}\right)^n \quad (9)$$

where K (with unit of m^{-1}) is the parameters reflecting the characteristics of slope displacement, and n is the material constants, P_a is the atmospheric pressure with a constant of 101.325 kPa, σ_i is the normal stress on the base of slice i, and $\sigma_i = N_i / (d_i \sec\alpha_i)$.

In Eq. (9), n typically varies between 0.3 and 0.8 for the clayey soil (Duncan and Chang 1970). Corresponding to the soft clayey soil, a small value is given for K, and a large value is given for n in their range, which indicates that a large displacement would be yielded.

According to the strength reduction technique and the definition of the slope FOS, the relationship between the shear stress (τ_i) and shear strength (τ_f) in slice i can be defined as follows:

$$\tau_i = \frac{\tau_f}{F_s} \quad (10)$$

where F_s is the slope FOS.

Because slope sliding is the result of the shear failure of the slip surface, which is subjected to the Mohr-Coulomb (M-C) strength criterion, the shear strength (τ_f) in slice i satisfies as follows:

$$\tau_f = c + \frac{N_i}{d_i \sec\alpha_i}\tan\varphi \quad (11)$$

where c is the soil cohesion, and φ is the soil internal friction angle.

The relationship between the shear stress and shear strength of the slip surface expressed by Eq. (10) is substituted into Eq. (8). Moreover, τ_i is replaced by (τ_f / F_s) on the left side of Eq. (8), and τ_f is replaced by ($\tau_i F_s$) on the right side of Eq. (8). Thus, Eq. (8) is rewritten as follows:

$$\tau_i = \tau_f \frac{1}{F_s}\left(\frac{a_i}{F_s \Delta_0}\cos\alpha_i + \frac{b_i}{F_s}\right) \quad (12)$$

It should be noted that compared to Eq. (8), the shear

stress expressed by Eq. (12) would vary by not only the horizontal slope displacement but also the slope FOS. Thus, in the subsequent derivation process, the horizontal slope displacement would be embedded into the formula of the slope FOS, and the calculation of the horizontal slope displacement is also related to the slope FOS. Thus, the coupling calculation between the slope FOS and horizontal slope displacement is needed in the present method.

Substituting $S_i = \tau_i d_i \sec\alpha_i$ into Eq. (12) and using Eq. (11) to calculate the shear strength, the formula for calculating the shear force (S_i) on the base of slice i can be thus converted into:

$$S_i = \frac{1}{F_s}\cdot\left(\frac{a_i\cdot\cos\alpha_i}{F_s\Delta_0}+\frac{b_i}{F_s}\right)\cdot(cd_i\sec\alpha_i + N_i\cdot\tan\varphi) \tag{13}$$

Substituting Eq. (6) into Eqs. (4) and (5) and combined with Eq. (13) yields as follows:

$$\begin{aligned}&[(\sin\alpha_i-\lambda f_i\cos\alpha_i)\left(\frac{a_i\cos\alpha_i}{F_s\Delta_0}+\frac{b_i}{F_s}\right)\tan\varphi+\\&(\cos\alpha_i+\lambda f_i\sin\alpha_i)F_s]E_i=\\&[(\sin\alpha_i-\lambda f_{i-1}\cos\alpha_i)\left(\frac{a_i\cos\alpha_i}{F_s\Delta_0}+\frac{b_i}{F_s}\right)\tan\varphi+\\&(\cos\alpha_i+\lambda f_{i-1}\sin\alpha_i)F_s]E_{i-1}-F_sT_i+R_i\end{aligned} \tag{14}$$

where

$$T_i = (W_i - k_V W_i + Q_y)\sin\alpha_i + (k_H W_i - Q_x)\cos\alpha_i \tag{15}$$

$$R_i = \left(\frac{a_i\cos\alpha_i}{F_s\Delta_0}+\frac{b_i}{F_s}\right)\times\begin{Bmatrix}cd_i\sec\alpha_i+\\[(W_i-k_VW_i+Q_y)\cos\alpha_i-\\(k_HW_i+Q_x)\sin\alpha_i-U_i]\tan\varphi\end{Bmatrix} \tag{16}$$

Using Eq. (14), the recurrence equation for the interslice normal force (E_i) can be obtained as follows:

$$\Phi_i E_i = \Phi_{i-1}E_{i-1}\psi_{i-1} + F_sT_i - R_i \tag{17}$$

In Eq. (17), the calculation formulas of Φ_i, $\Phi_{i\text{-}1}$, and $\psi_{i\text{-}1}$ can be calculated as follows:

$$\begin{aligned}\Phi_i = &(\sin\alpha_i-\lambda f_i\cos\alpha_i)\left(\frac{a_i\cos\alpha_i}{F_s\Delta_0}+\frac{b_i}{F_s}\right)\tan\varphi+\\&(\cos\alpha_i+\lambda f_i\sin\alpha_i)F_s\end{aligned} \tag{18}$$

$$\begin{aligned}\Phi_{i-1} = &(\sin\alpha_{i-1}-\lambda f_{i-1}\cos\alpha_{i-1})\left(\frac{a_{i-1}\cos\alpha_{i-1}}{F_s\Delta_0}+\frac{b_{i-1}}{F_s}\right)\tan\varphi\\&+(\cos\alpha_{i-1}+\lambda f_{i-1}\sin\alpha_{i-1})F_s\end{aligned} \tag{19}$$

$$\Psi_{i-1} = \begin{bmatrix}(\sin\alpha_i-\lambda f_{i-1}\cos\alpha_i)\times\\\left(\frac{a_i\cos\alpha_i}{F_s\Delta_0}+\frac{b_i}{F_s}\right)\tan\varphi+\\(\cos\alpha_i+\lambda f_{i-1}\sin\alpha_i)F_s\end{bmatrix}/\Phi_{i-1} \tag{20}$$

The recurrence equation for the interslice normal force (E_i) expressed by Eq. (17) has the boundary conditions such that $E_0 = 0$ and $E_m = 0$. Therefore, the formula of the slope FOS is derived using Eq. (17). Here, the formula of the slope FOS has the same expression as the original LE M-P method as follows:

$$F_s = \frac{\sum_{i=1}^{m-1}\left(R_i\prod_{j=i}^{m-1}\psi_j\right)+R_m}{\sum_{i=1}^{m-1}\left(T_i\prod_{j=i}^{m-1}\psi_j\right)+T_m} \tag{21}$$

In Eq. (21), the parameters ψ_i and R_i (i.e., Eqs. (17)-(20)) are related to the slope FOS (F_s). Hence, Eq. (21) is an implicit formula for the slope FOS, and the iterative loop strategy is required to calculate the slope FOS.

The parameter λ, which is adopted to describe the relationship between the interslice forces in the M-P method, can be determined according to the moment equilibrium condition at the midpoint of the slip surface for all forces in slice i. As shown in Fig. 1, let $M_i = E_i z_i$ and $M_{i\text{-}1} = E_{i\text{-}1}z_{i\text{-}1}$. The moment equilibrium condition for all the forces around the midpoint f of the slip surface in slice i can be given as follows:

$$\begin{aligned}M_i = &M_{i-1}+\lambda\frac{d_i}{2}(f_iE_i+f_{i-1}E_{i-1})-\\&\frac{d_i}{2}(E_i+E_{i-1})\tan\alpha_i-k_HW_i\frac{h_i}{2}+Q_xh_i\end{aligned} \tag{22}$$

Eq. (22) is the recurrence equation for the interslice moment (M_i). Then, based on the boundary conditions (i.e., $M_0 = 0$ and $M_m = 0$), the formula for the parameter λ is derived as follows:

$$\lambda = \frac{\sum_{i=1}^{m}\left[d_i(E_i+E_{i-1})\tan\alpha_i + k_H W_i h_i - 2Q_x\cdot h_i\right]}{\sum_{i=1}^{m}\left[d_i\left(f_iE_i+f_{i-1}E_{i-1}\right)\right]} \tag{23}$$

2.2 Solution of horizontal slope displacement in the expanded LE M-P method

As mentioned above, for a stable slope, the horizontal slope displacement is very small. Thus, the horizontal slope displacement Δ_0 can be solved according to the energy equation satisfied by the slope sliding body. As internal force, the force between slices has opposite directions. In addition, the adjacent slices remain in the close contact with the same absolute displacement but no relative displacement under a small slope displacement for a rigid body. Therefore, it can be approximately considered that the works done by the interslice forces are zero. For the energy done by the shear force on the slip surface, it should be given by the integral of the product force-displacement from zero to the final displacement value (i.e., Δ_i for slice i in Eq. (3)) for the reason that the shear force (calculated by $\tau_i d_i/\cos\alpha_i$ for slice i) is a function of the shear displacement based on the relationship between the shear stress (τ_i) and shear displacement expressed by Eq. (7). Therefore, the energy equation of the slope sliding body is obtained as follows:

$$\sum_{i=1}^{m}[(1-k_V)W_i+Q_y]\Delta_0\tan\alpha_i+\sum_{i=1}^{m}(k_HW_i-Q_x)\Delta_0-\sum_{i=1}^{m}\int_0^{\Delta_i}\tau_i\frac{d_i}{\cos\alpha_i}d\Delta=0 \tag{24}$$

In Eq. (24), the change of the inclination angle (i.e., α_i for slice i) of slip surface under slight displacement is neglected. Moreover, Eq. (24) can be satisfied under both the linear slip surface and curved slip surface because the energy, as a scalar independent of the tangency of the slip surface, is the sum of the work done by all external forces on the slope sliding body.

For the energy done by the shear force on the slip surface (i.e., the last term in the left-hand side of Eq. (24)), substituting Eq. (3) and Eq. (7) into the energy calculation of shear force and combined with Eq. (8) yields as follows:

$$\begin{aligned}\int_0^{\Delta_i}\tau_i\frac{d_i}{\cos\alpha_i}d\Delta&=\int_0^{\Delta_0/\cos\alpha_i}\frac{\Delta}{a'+b'\Delta}\frac{d_i}{\cos\alpha_i}d\Delta\\&=\frac{\tau_f}{b_i}\left[\frac{\Delta_0}{\cos\alpha_i}-\frac{a_i}{b_i}\ln\left(1+\frac{b_i\Delta_0}{a_i\cos\alpha_i}\right)\right]\frac{d_i}{\cos\alpha_i}\end{aligned} \tag{25}$$

To obtain an explicit formula for the horizontal slope displacement from Eq. (24), Eq. (8) is converted into:

$$a_i\tau_i\cos\alpha_i=\Delta_0\tau_f-b_i\Delta_0\tau_i \tag{26}$$

Substituting the relationship between the shear stress and the shear strength expressed by Eq. (10) into Eq. (26) and replacing τ_i on the right side of Eq. (26) with (τ_f / F_s), Eq. (26) can be rewritten as follows:

$$\tau_i=\tau_f\frac{\Delta_0\left(F_s-b_i\right)}{a_iF_s\cos\alpha_i} \tag{27}$$

Compared to Eq. (12), Eq. (27) is another expression of the shear stress, and it can better reflect the relationship among the shear stress, slope FOS, and horizontal slope displacement. In addition, Eq. (27) is used to derive the formula of the horizontal slope displacement to ensure that the obtained horizontal slope displacement is greater than zero when the slope FOS is greater than b_i (i.e., the calculated shear stress is less than the actual shear strength). Then, replacing τ_f on the right side of Eq. (27) with (τ_i F_s), Eq. (27) can be rewritten as follows:

$$\frac{\Delta_0}{a_i\cos\alpha_i}=\frac{1}{F_s-b_i} \tag{28}$$

Substituting Eqs. (27) and (28) into Eq. (25), Eq. (25) can be rewritten as follows:

$$\int_0^{\Delta_i}\tau_i\frac{d_i}{\cos\alpha_i}d\Delta=\tau_fd_i\frac{\Delta_0(F_s-b_i)}{a_ib_i\cos^2\alpha_i}\left[\frac{\Delta_0}{\cos\alpha_i}-\frac{a_i}{b_i}\ln\left(\frac{F_s}{F_s-b_i}\right)\right] \tag{29}$$

Thereafter, calculating the shear strength (τ_f) in Eq. (29) with Eq. (11) and subsequently substituting Eq. (29) into Eq. (24), thereby the explicit formula of the horizontal slope displacement can be deduced as follows:

$$\Delta_0=\frac{\left\{\begin{aligned}&\sum_{i=1}^{m}[(1-k_V)W_i+Q_y]\tan\alpha_i+\sum_{i=1}^{m}(k_HW_i-Q_x)+\\&\sum_{i=1}^{m}\frac{F_s-b_i}{b_i^2\cos\alpha_i}\ln\left(\frac{F_s}{F_s-b_i}\right)(cd_i\sec\alpha_i+N_i\tan\varphi)\end{aligned}\right\}}{\sum_{i=1}^{m}\frac{F_s-b_i}{a_ib_i\cos^2\alpha_i}(cd_i\sec\alpha_i+N_i\tan\varphi)} \tag{30}$$

Eq. (30) shows that the horizontal slope displacement Δ_0 can be obtained after solving F_s (i.e., Eq. (21)) and N_i (i.e., Eq. (4)). From Eq. (30), it can be known that the horizontal slope displacement (Δ_0) is positive when $F_s > b_i$, and it would approach infinity as F_s approaches b_i, where b_i is the failure ratio R_f and R_f is chosen to reflect the relationship between the selected shear strength and actual shear strength of the soil.

It should be noted that the displacement of sliding body is actually the result of slope deformation (such as the displacement of slope surface calculated by the numerical simulation software FLAC^{3D} in slope example 1). In the LE methods, the slope displacement is regarded as the result of movement of the whole sliding body along the slip surface because of the assumption of the rigid sliding body, and the slip surface could be any shaped slip surface as the traditional M-P method deals with. Moreover, the slices in the sliding body are not deformed. Nevertheless, the displacement compatibility condition between slices (i.e., Eq. (2)) need be satisfied whatever type of slip surface it is. Thus, despite the strain energy from the slope deformation does not need to be considered, the forces acting on the sliding body would require energy due to the displacement of the rigid sliding body. Furthermore, under the assumption of the rigid sliding body, it would become simple to solve the slope displacement in the LE methods using the energy equation of sliding body regardless of the strain energy from the slope deformation. In addition, for a slope in a stable state, its displacement is often smaller than its size. Thereby, it is feasible to treat the slope sliding as the overall movement of the rigid sliding body under the small slope displacement.

2.3 Flow chart of slope stability analysis with the double solutions of the slope FOS and horizontal slope displacement

According to the above analysis, the iterative loop calculations of the slope FOS and parameter λ should be adopted to solve for the LE stability of the slope and calculate the horizontal slope displacement in the extended LE M-P method based on the force-displacement coupled mode. The flow chart for LE analysis of the slope stability with the double solutions of the slope FOS and horizontal slope displacement is shown in Fig. 3. To give the distinguish steps of the numerical simulation method (such as the finite element method or finite difference method) and LE method, the flowchart for the calculation of the

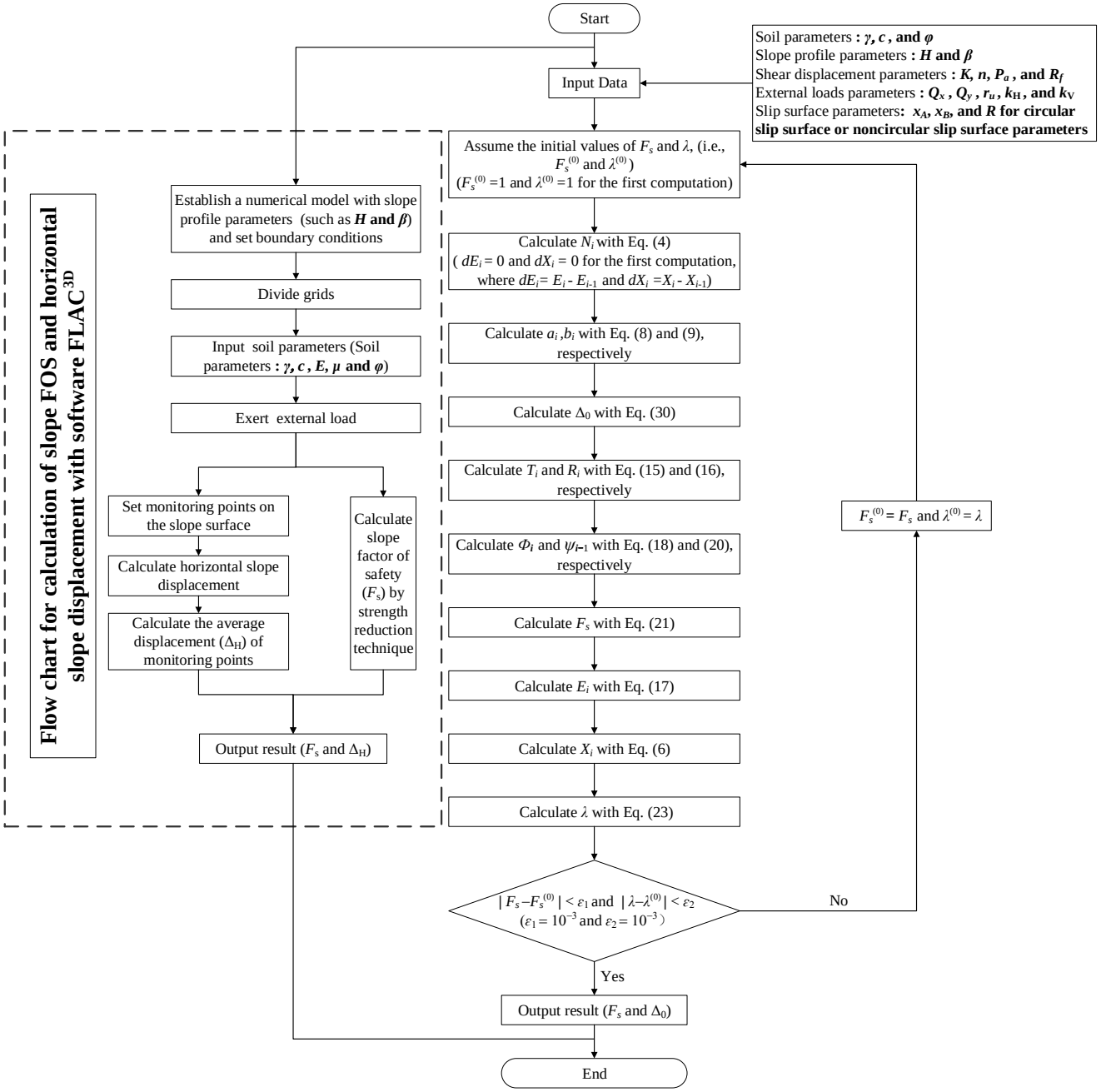

Fig. 3 Flow chart for LE analysis (or the software FLAC3D) on the slope stability with the double solutions of the slope FOS and horizontal slope displacement

slope stability and slope displacement using the software FLAC3D is also listed in Fig. 3. It should be noted that the displacement of sliding body is from the slope deformation under the gravity and external force in the numerical simulation method. However, the appearance of slope displacement in the present method is due to the movement of the rigid sliding body, and the compatible condition of displacement between slices and the constitutive relation of the shear displacement and shear stress on the slip surface should be adopted to obtain the slope displacement. Despite the calculation mode on the slope displacement for the present method and numerical simulation method is different, the results from the following slope example 1 reflect that the obtained curves of the slope displacement vs. the slope FOS by the two methods are similar and close to each other. Thus, the rationality and feasibility of the present method is verified.

In the flow chart of Fig. 3, five groups (i.e., the slope profile parameters, soil parameters, external loads parameters, slip surface parameters, and shear displacement parameters) as for the input step could be classified according to the properties of parameters. Compared with the traditional LE methods, only the shear displacement parameters are increased in the present method to get the additional result (i.e., the horizontal slope displacement). Moreover, the input of the shear displacement parameters (except for the parameters required in the traditional LE methods) in the present method does not bring complexity

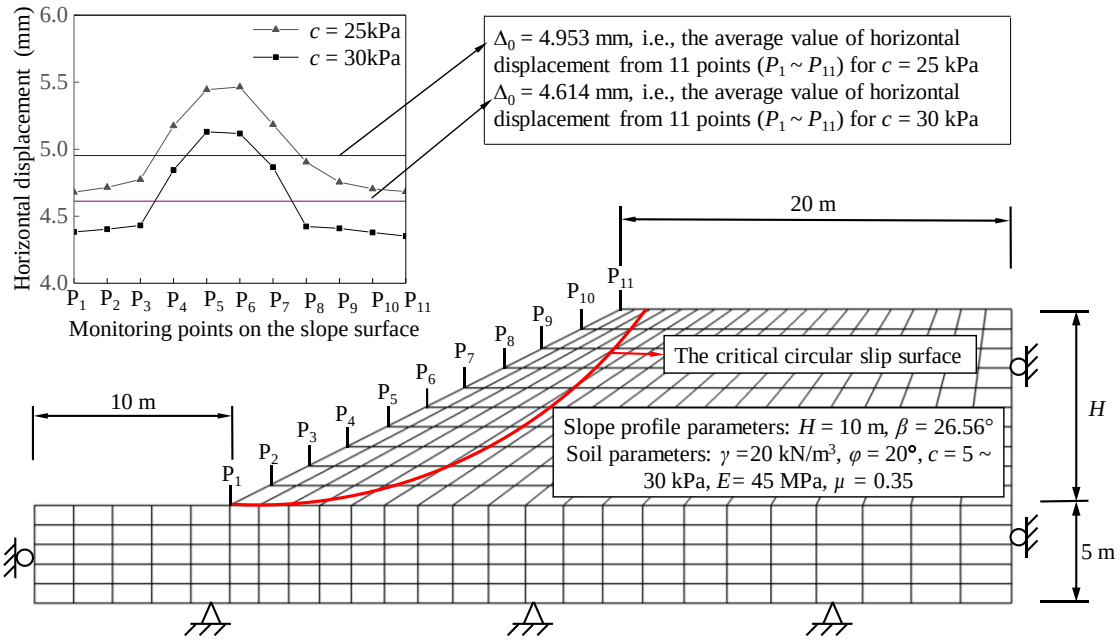

Fig. 4 Slope example 1

Table 1 Comparison of results for slope stability in slope example 1

Case	Slope height	Slope angle	Soil parameters			Calculated results					
			Unit weight	Cohesion	Internal friction angle	Minimum Slope FOS			Horizontal slope displacement Δ_0 (mm)		
	H (m)	β (°)	γ (kN / m^3)	c (kPa)	φ (°)	FLAC3D	Present method	Diff (%)	FLAC3D	Present method	Diff (%)
1	10	26.56°	20.0	5	19.6	1.090	1.098	0.73%	8.718	9.035	-3.64%
2	10	26.56°	20.0	10	19.6	1.348	1.354	0.45%	6.823	7.083	-3.81%
3	10	26.56°	20.0	15	19.6	1.574	1.583	0.57%	5.986	6.158	-2.87%
4	10	26.56°	20.0	20	19.6	1.777	1.784	0.39%	5.321	5.496	-3.29%
5	10	26.56°	20.0	25	19.6	1.984	1.989	0.25%	4.953	4.953	0.00%
6	10	26.56°	20.0	30	19.6	2.164	2.170	0.28%	4.614	4.614	0.00%

to the program of the slope stability analysis. Hence, the present method has the same simplicity with the traditional LE methods for users.

3. Comparison and analysis of slope examples

3.1 Comparison with the numerical method

Slope example 1: As shown in Fig. 4, the slope example is given by Rocscience Inc. (2003) with a slope height H = 10 m and a slope angle β = 26.57°. The soil parameters of the slope have a unit weight of γ = 20.0 kN/m^3 and an internal friction angle of φ = 19.6°. To verify the feasibility of the present method, the corresponding numerical model with an elastic modulus E = 45 MPa and a Poisson's ratio μ = 0.35 is established in the software FLAC3D (Itasca Consulting Group 2012) to obtain the numerical results of the horizontal displacement of the slope surface. Since the critical slip surface of the slope is near the slope surface, 11 points (from P1 to P11 shown in Fig. 4) are set on the slope surface to obtain the numerical results of the horizontal displacement of the slope surface. Meanwhile, the slope horizontal displacement is calculated by the software FLAC3D without the use of the strength reduction technique. The main reason is that the slope displacement is the result of the deformation of slope under the gravity and external loads without accompanying by the reduction of geotechnical strength. The strength reduction technique is applied to reduce the geotechnical strength so as to let the slope appear plastic flow reflecting the slope instability, and the slope FOS is then obtained. As the average horizontal slope displacement is obtained by the present method under the assumption that the slope sliding is regarded as rigid, the numerical results of the horizontal displacement from these 11 points on the slope surface are also averaged. Fig. 4 shows the numerical results of the horizontal displacement from these 11 points on the slope surface and their average value when the soil cohesion is c = 25 kPa and 30 kPa. Based on the average value of the numerical results of the horizontal displacement for c = 25 kPa and 30 kPa, the displacement parameters (i.e., K and n) would be calculated by the binary search method after several slope stability analyses. Thus, K = 71.88 m^{-1} and n = 0.294 for R_f

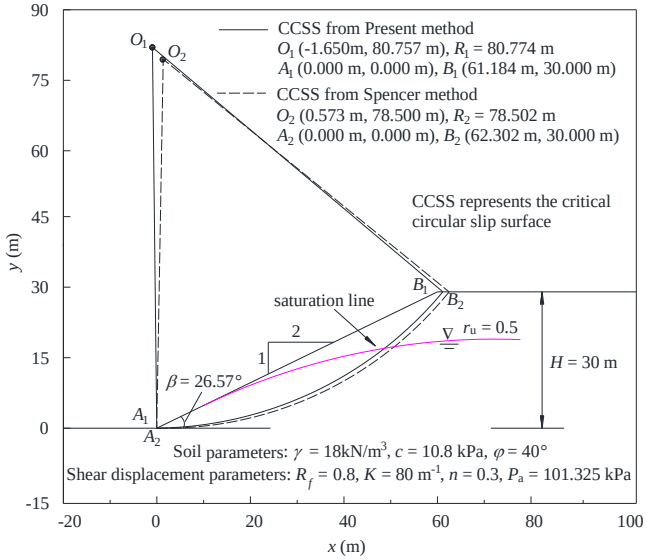

Fig. 5 Slope example 2

Table 2 Comparison of results for slope stability in slope example 2

Calculation method		Minimum slope FOS	Horizontal slope displacement Δ_0 (mm)
Rocscience Inc. (2003)	Spencer method	1.01	—
	Spencer method	1.02	—
	Spencer method	1.08	—
Janbu Simplified method (Janbu 1973)		1.01	—
GLE method (Fredlund *et al.* 1981)		1.05	—
GLE method (Enoki *et al.* 1990)		1.06	—
Bishop method (Bishop 1955)		1.03	—
GeoStudio 2012		1.04	—
M-P method (Morgenstern and Price 1965)		1.08	—
Present method		1.06	24.74

= 0.8 and P_a =101.325 kPa in the theoretical model of the present method. Thereafter, c is given as 5 kPa, 10 kPa, 15 kPa, and 20 kPa to contrast the results from the present method and numerical method in Table 1, where the numerical results of the slope displacement are the average value of horizontal displacements from 11 points on slope surface. Additionally, it should be noted that the critical slip surface shown in Fig. 4 is only a schematic diagram.

From Table 1 and Fig. 4, it can be known that in terms of the minimum slope FOS and horizontal slope displacement, the present method has close results with the numerical method, indicating the reasonability of the present method.

3.2 Comparison with traditional LE methods

Slope example 2: As shown in Fig. 5, which is from the slope case with the pore water pressure given by Rocscience Inc. (2003), the slope has a height H = 30 m and

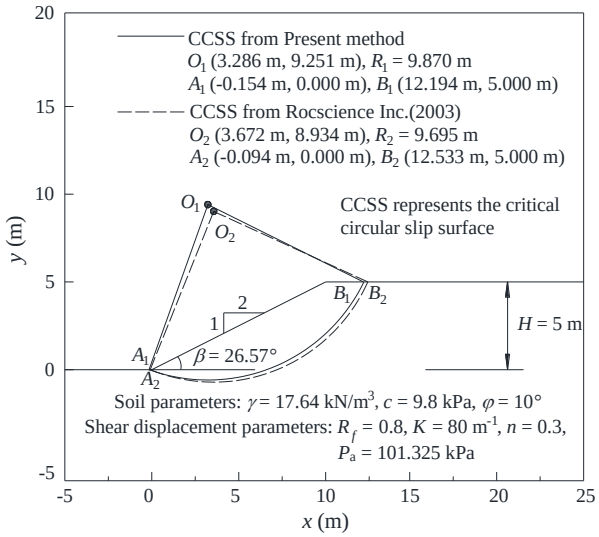

Fig. 6 Slope example 3

Table 3 Comparison of results for slope stability in slope example 3

Calculation method		Minimum slope FOS	Horizontal slope displacement Δ_0 (mm)
Rocscience Inc. (2003)	Bishop method	1.344	—
	Ordinary method	1.278	—
	Bishop Simplified method	1.348	—
	Fellenius / Ordinary method	1.282	—
Janbu method (Janbu 1973)		1.340	—
M-P method (Morgenstern and Price 1965)		1.341	—
Spencer method (1969)		1.341	—
GLE method (Fredlund *et al.* 1981)		1.339	—
GLE method (Enoki et al 1990)		1.343	—
GeoStudio 2012		1.335	—
FLAC3D		1.337	—
Huang's method (Huang 2013)		1.304	5.87
Present method		1.334	5.65

a slope angle β = 26.57°. The soil parameters of the slope have a unit weight of γ = 18.0 kN/m^3, a cohesion of c = 10.8 kPa, and an internal friction angle of φ = 40°. The pore water force that acts on the sliding body is modeled using the pore-water pressure coefficient r_u with a value of 0.5. Based on the reasonable range of the parameters listed above, the shear displacement parameters of the soil are given as follows: R_f = 0.8, n = 0.3, K = 80 m^{-1}, and P_a =101.325 kPa. Then, through the LE analysis of slope stability, the calculation results are shown in Table 2 and the critical circular slip surface of the slope is shown in Fig. 5. Furthermore, the numerical result from the software GeoStudio (GeoStudio 2012) is also given to verify the rationality of the present method. In Fig. 5, the solid line is the critical circular slip surface obtained by the present method, and the dashed line is the critical circular slip surface obtained from the Spencer method. A similar

representation for the critical slip surface used in slope example 2 is also applicable in the following slope example 3.

From Table 2 and Fig. 5, it can be known that (1) compared to the traditional LE methods (such as the Bishop method, M-P method, and GLE method) and numerical simulation method from the software GeoStudio, the results of the minimum slope FOS and the critical slip surface obtained by the present method are also quite close, further indicating the feasibility of the present method; and (2) superior to the traditional LE M-P method, the present method can calculate the double solutions of the slope FOS and horizontal slope displacement.

3.3 Comparison with Huang's method

Slope example 3: As shown in Fig. 6, the slope has a slope height of H = 5 m and a slope angle of β = 26.57° from Rocscience Inc. (2003). The soil parameters of the slope have a unit weight of γ = 17.64 kN/m^3, a cohesion of c = 9.8 kPa, and an internal friction angle of φ = 10°. Here, the shear displacement parameters of the soil are taken as follows: R_f = 0.8, n = 0.3, K = 80 m^{-1}, and P_a =101.325 kPa. Through LE analysis of slope stability, the calculation results obtained by the traditional LE method (such as the Bishop method, Janbu method, M-P method, and GLE method), Huang's method (Huang 2013), and the present method are shown in Table 3. The obtained critical circular slip surface of the slope is shown in Fig. 6. In addition, the numerical results from the software GeoStudio and FLAC3D are also given for further verification.

From Table 3, it can be known that compared with Huang's method (corresponding to the Janbu method), the slope FOS obtained by the present method (corresponding to the M-P method) is larger, but it is closer to the results obtained by the rigorous LE methods, such as the GLE method. Furthermore, the horizontal slope displacement obtained by Huang's method is slightly larger than the present method. The main reason for this difference is that additional conditions (i.e., the energy equation satisfied by the slope sliding body) beyond the mechanical equilibrium conditions are adopted by the present method to solve the horizontal slope displacement. In the present method, the double solutions of the slope FOS and horizontal slope displacement are computed to analyze the slope stability. However, Huang's method separately calculates the slope FOS and horizontal slope displacement, and the slope FOS should be obtained before the horizontal slope displacement is solved. In addition, Huang's method inherits the deficiency that the calculation convergence is worse with the increase in the number of divided slices in the traditional Janbu method as a result of the discontinuity of the first derivative of the interslice moment. However, the convergence problem can be solved well in the present method by using the assumption of the interslice forces from the M-P method.

4. Analysis of the effect of shear displacement parameters on slope stability

4.1 The effect of n on the slope FOS and horizontal slope displacement

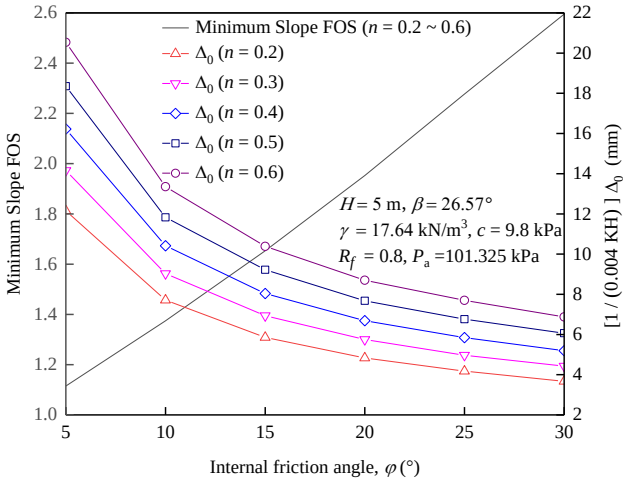

(a) Curve of minimum slope FOS or horizontal slope displacement vs. internal friction angle

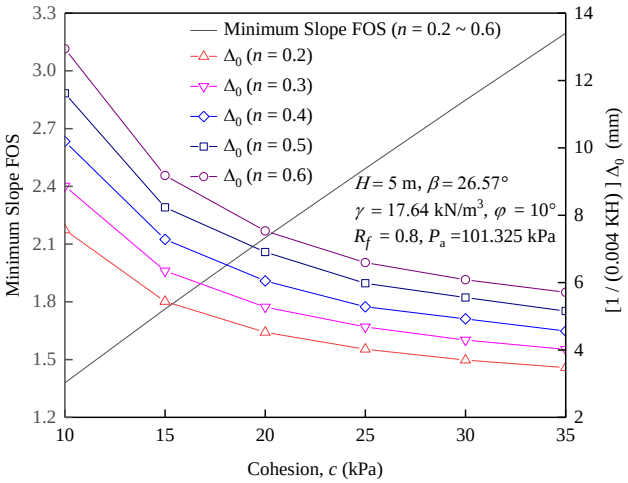

(b) Curve of minimum slope FOS or horizontal slope displacement vs. cohesion

Fig. 7 Curves of minimum slope FOS and horizontal slope displacement vs. shear strength parameters for different n

When the shear displacement parameter n is 0.2, 0.3, 0.4, 0.5 and 0.6, the curves of the slope FOS or the horizontal slope displacement vs. the internal friction angle are shown in Fig. 7(a) (here c = 9.8 kPa), and the curves of the slope FOS or the horizontal slope displacement vs. the cohesion are shown in Fig. 7(b) (here φ = 10°). In Fig. 7, the parameter n mainly affects the horizontal slope displacement and has a limited influence on the minimum slope FOS, indicating that the shear displacement parameter would have a direct influence on the horizontal slope displacement but basically does not lead to the change of the slope stability. Therefore, the same curve for different n is used to represent the variation of the minimum slope FOS with the shear strength parameters.

From Fig. 7, it should be known that (1) with the increase of the shear displacement parameter n, the horizontal slope displacement increases; (2) with the decrease of the shear strength parameters (i.e., φ and c), the horizontal slope displacement gradually increases and the minimum slope FOS gradually decreases, implying that the

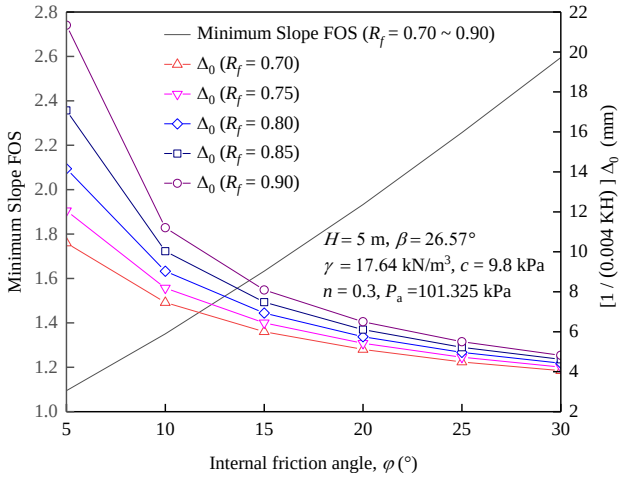

(a) Curve of minimum slope FOS or horizontal slope displacement vs. internal friction angle

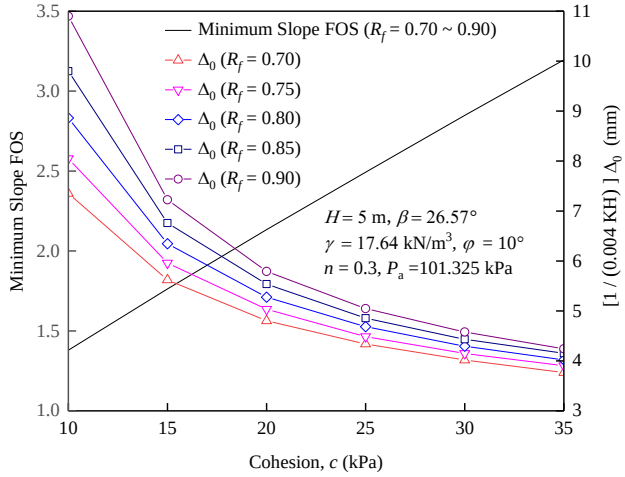

(b) Curve of minimum slope FOS or horizontal slope displacement vs. cohesion

Fig. 8 Curves of minimum slope FOS and horizontal slope displacement vs. shear strength parameters for different R_f

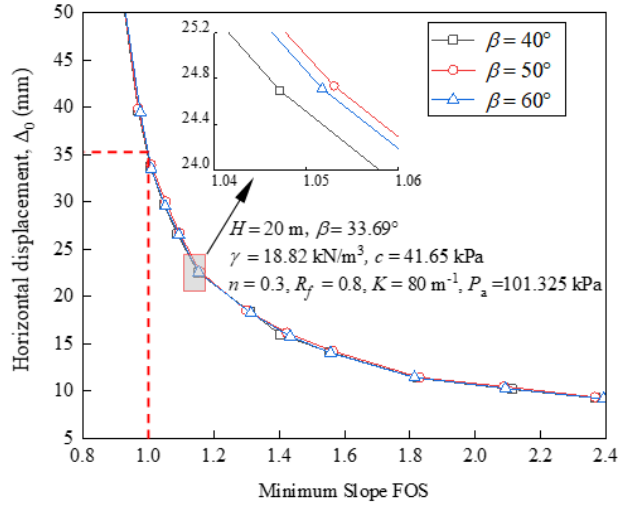

Fig. 9 Curves of horizontal slope displacement vs. minimum slope FOS

slope would have a larger sliding displacement when the slope tends to be unstable; and (3) the horizontal slope displacement has a negative linear proportional relation with the displacement parameter K (i.e., the horizontal slope displacement linearly decreases with the increase of K), and thereby the horizontal slope displacement under different K can be converted by the horizontal slope displacement Δ_0 when $K = 250 / H$.

It should be noted that the influence of the parameter n on the horizontal slope displacement is due to the variation of k_{initial} with n in Eq. (7). The effect of the parameter n as an exponent on k_{initial} depends on the constant term (σ_i / P_a). Hence, the influence of the parameter n on the horizontal slope displacement is different under the different cases. If the normal stress (σ_i) is less than P_a, k_{initial} decreases and the horizontal slope displacement increases with the increase of n; otherwise, the opposite results are found.

4.2 The effect of R_f on the slope FOS and horizontal slope displacement

When the parameter R_f is 0.70, 0.75, 0.80, 0.85 and 0.90, the curves of the slope FOS or the horizontal slope displacement vs. the internal friction angle are shown in Fig. 8(a) (here c = 9.8 kPa), and the curves of the slope FOS or the horizontal slope displacement vs. the cohesion are shown in Fig. 8(b) (here φ = 10°). In Fig. 8, the same curve for a different R_f is used to represent the variation of the minimum slope FOS with the shear strength parameters because the parameter R_f mainly affects the horizontal slope displacement and has a limited influence on the minimum slope FOS.

Fig. 8 shows that (1) with the decrease in the shear strength parameters (i.e., c and φ), the minimum slope FOS gradually increases and the horizontal slope displacement gradually decreases; and (2) with the increase in R_f, the horizontal slope displacement increases.

4.3 The relationship between the horizontal slope displacement and slope FOS

In practical engineering, the slope displacement could provide direct and reliable information to reflect the state of a slope. Moreover, the slope would tend to be unstable with increases in the slope displacement. However, the current research on slope displacement mainly adopts a qualitative description, which could not satisfy the needs of the quantitative analysis. Therefore, it is necessary to reveal the relationship between the slope FOS and slope displacement. In this case, a slope is given with a slope of height H = 20 m. The soil parameters of the slope have a unit weight of γ = 18.82 kN/m^3, a cohesion of c = 41.65 kPa, and an internal friction angle of φ = 15°. The shear displacement parameters of the soil are taken as follows: R_f = 0.8, n = 0.3, K = 80 m^{-1}, and P_a =101.325 kPa. For the actual artificial slope, the slope ratio is usually taken as 1: 0.5 ~ 1: 2, which means that the slope angle is approximately 30° ~ 60°. Then, the curves of the horizontal slope displacement vs. the slope FOS is here studied with the slope angle varying from 40° ~ 60°. When the slope angle β is 40°, 50°, and 60°, the slope stability is analyzed with the variation of the internal friction angle from 40° to 0°, and the curves of the

horizontal slope displacement vs. the slope FOS are drawn in Fig. 9. The variation of the internal friction angle from 40° to 0° reflects the reduction of the resisting ability of the slope. Certainly, it is also possible to increase the external loads to enlarge the sliding force of the slope.

Fig. 9 shows that the curves of the horizontal slope displacement vs. the slope FOS are very close to each other under different slope angles. Furthermore, the curve of the horizontal slope displacement vs. the slope FOS could be approximated by a hyperbola with a high degree of accuracy. If some monitoring points are evenly arranged on the slope surface to obtain the real-time horizontal slope displacement (Pei *et al.* 2019), the curve of the horizontal slope displacement vs. the slope FOS is also obtained by calculating the average value of the horizontal slope displacements of these monitoring points and analyzing the corresponding slope stability. Then, the approximate formula of the horizontal slope displacement related to the slope FOS would be obtained with the hyperbolic model by the curve fitting method on the measured curve of the horizontal slope displacement vs. the slope FOS. By applying this approximate formula, the critical horizontal slope displacement ($\Delta_{critical}$) for the minimum slope FOS equal to 1.000 can be calculated. Thereafter, the critical horizontal slope displacement can be combined with the subsequent measured horizontal slope displacement to determine whether the slope is unstable. In other words, the slope would be in an unstable state when the average value of the real-time horizontal slope displacements of these monitoring points is larger than $\Delta_{critical}$, and a warning can be given in advance. Thus, these curves in Fig. 9 provide a theoretical basis for predicting landslides, which also demonstrates the applicability of the present method (i.e., the extended LE M-P method based on the force-displacement coupled mode).

5. Conclusions

Based on the force-displacement coupled mode, this work expanded the LE M-P method. Except for the mechanical equilibrium conditions of a sliding body adopted in the traditional LE M-P method, the present method introduced a nonlinear model of the shear stress and shear displacement and applied the energy equation satisfied by a sliding body under a small displacement. Therefore, double solutions of the slope FOS and horizontal slope displacement were obtained. By the comparison and analysis of slope examples, the feasibility of the present method is verified. Meanwhile, the following conclusions were obtained:

• The displacement parameters of the soil affect the horizontal slope displacement but have a limited effect on the slope FOS.

• The horizontal slope displacement increases with the decrease of the shear displacement parameter K, and the influence of the shear displacement parameter n on the horizontal slope displacement depends on the ratio of the normal stress (σ_i) to the atmospheric pressure (P_a).

• The curves of the horizontal slope displacement vs. the minimum slope FOS could be fitted by the hyperbolic model, which would be beneficial to obtain the horizontal slope displacement for the slope in the critical state and provides a theoretical basis for early warning on slope collapse by combining the measured horizontal slope displacement on the slope surface.

Acknowledgments

The research described in this paper was financially supported by the National Natural Science Foundation of China (Grant No. 51608541) and the Natural Science Foundation of Hunan Province, China (Grant No. 2019JJ50772).

References

Atkinson, J.H. (1981), *Foundations and Slopes: An Introduction to Applications of Critical State Soil Mechanics*, McGraw-Hill, London, U.K.

Bai, T., Qiu, T., Huang, X.M. and Li, C. (2014), "Locating global critical slip surface using the Morgenstern-Price method and optimization technique", *Int. J. Geomech.*, **14**(2), 319-325. https://doi.org/10.1061/(ASCE)GM.1943-5622.0000312.

Bishop, A.W. (1955), "The use of the slip circle in the stability analysis of slopes", *Géotechnique*, **5**(1), 7-17. https://doi.org/10.1680/geot.1955.5.1.7.

Chen, Z.Y. and Morgenstern, N.R. (1983), "Extensions to the generalized method of slices for stability analysis", *Can. Geotech. J.*, **20**(1), 104-119. https://doi.org/10.1139/t83-010.

Cheng, H. and Zhou, X.P. (2015), "A novel displacement-based rigorous limit equilibrium method for three-dimensional landslide stability analysis", *Can. Geotech. J.*, **52**(12), 2055-2066. https://doi.org/10.1139/cgj-2015-0050.

Deng, D.P., Lu, K. and Li, L. (2019), "LE analysis on unsaturated slope stability with introduction of nonlinearity of soil strength", *Geomech. Eng.*, **19**(2), 179-191. http://doi.org/10.12989/gae.2019.19.2.179.

Duncan, J.M. and Chang, C.Y. (1970), "Nonlinear analysis of stress and strain in soils", *J. Soil Mech. Found. Div.*, **96**(5), 1629-1653.

Enoki, M., Yagi, N. and Yatabe, R. (1990), "Generalized slice method for slope stability analysis", *Jap. Soc. Soils Mech. Found.*, **30**, 1-13. http://doi.org/10.3208/sandf1972.30.2.1.

Fredlund, D.G., Krahn, J. and Pufahl, D.E. (1981). "Relationship between limit equilibrium slope stability methods", *Proceedings of 10th International Conference on Soil Mechanics and Foundation Engineering*, Stockholm, Sweden, June.

GeoStudio (2012), Geo-Slope International Ltd., Calgary, Alberta, Canada.

Ghanbari, A., Khalilpasha, A., Sabermahani, M. and Heydari, B. (2013), "An analytical technique for estimation of seismic displacements in reinforced slopes based on horizontal slices method (HSM)", *Geomech. Eng.*, **5**(2), 143-164. http://doi.org/10.12989/gae.2013.5.2.143.

Gong, B. and Tang C.A. (2016), "Slope-slide simulation with discontinuous deformation and displacement analysis", *Int. J. Geomech.*, **17**(5), E4016017. https://doi.org/10.1061/(ASCE)GM.1943-5622.0000746.

Guo, M.W., Liu, S.J., Wang, S.L. and Yin, S.D. (2020), "Determination of residual thrust force of landslide using vector sum method", *J. Eng. Mech.*, **146**(7), 04020063. https://doi.org/ 10.1061/(ASCE)EM.1943-7889.0001791.

Himanshu, N., Kumar, V., Burman, A., Maity, D. and Gordan, B.

(2019), "Grey wolf optimization approach for searching critical failure surface in soil slopes", *Eng. Comput*., 1-14. https://doi.org/10.1007/s00366-019-00927-6.

Huang, C.C. (2013), "Developing a new slice method for slope displacement analyses", *Eng. Geol*., **157**(5), 39-47. https://doi.org/10.1016/j.enggeo.2013.01.018.

Huang, C.C. (2014), "Force equilibrium-based finite displacement analyses for reinforced slopes: Formulation and verification", *Geotext. Geomembranes*, **42**(4), 394-404. https://doi.org/10.1016/j.geotexmem.2014.06.004.

Itasca Consulting Group. (2012), *FLAC3D 5.0 Manual*, Itasca Consulting Group, Minneapolis, Minnesota, U.S.A.

Janbu, N. (1973), *Slope Stability Computations*, in *Embankment Dam Engineering: Casagrande Memorial Volume*, John Wiley, New York, U.S.A., 47-86.

Kondner, R.L. (1963), "Hyperbolic stress-strain response: Cohesive soils", *J. Soil Mech. Found. Div*., **89**(1), 115-143.

Mandal, A.K., Li, X.P. and Shrestha, R. (2019), "Influence of water level rise on the bank of reservoir on slope stability: A case study of Dagangshan Hydropower Project", *Geotech. Geol. Eng*., **37**(6), 5187-5198. https://doi.org/10.1007/s10706-019-00972-4.

McCombie, P.F. (2009), "Displacement based multiple wedge slope stability analysis", *Comput. Geotech*., **36**(1), 332-341. https://doi.org/10.1016/j.compgeo.2008.02.008.

Mohtarami, E., JafariM, A. and Amini, M. (2014), "Stability analysis of slopes against combined circular-toppling failure", *Int. J. Rock Mech. Min. Sci*., **67**(4), 43-56. https://doi.org/10.1016/ j.ijrmms.2013.12.020.

Morgenstern, N.R. and Price, V.E. (1965), "The analysis of the stability of general slip surfaces", *Géotechnique*, **15**(1), 79-93. https://doi.org/10.1680/geot.1968.18.1.92.

Pei, H.F., Zhang, S.Q., Borana, L., Zhao, Y. and Yin, J.H. (2019), "Slope stability analysis based on real-time displacement measurements", *Measurement*, **131**(1), 686-693. https://doi.org/10.1016/j.measurement.2018.09.019.

Rocscience Inc. (2003), *Slide Verification Manual*, Rocscience Inc., Toronto, Canada, 8-118.

Siacara, A.T., Napa-Garcia, G.F., Beck, A.T. and Futai, M.M. (2020), "Reliability analysis of earth dams using direct coupling", *J. Rock Mech. Geotech. Eng*., **12**(2), 366-380. https://doi.org/10.1016/j.jrmge.2019.07.012.

Spencer, E. (1973), "Thrust line criterion in embankment stability analysis", *Géotechnique*, **23**(1), 85-100. https://doi.org/10.1680/geot.1973.23.1.85.

Sun, G.H., Cheng, S.G., Jiang, W. and Zheng, H. (2016), "A global procedure for stability analysis of slopes based on the Morgenstern-Price assumption and its applications", *Comput. Geotech*., **80**(12), 97-106. https://doi.org/10.1016/j.compgeo.2016.06.014.

Tran, A.T.P., Kim, A.R. and Cho, G.C. (2019), "Numerical modeling on the stability of slope with foundation during rainfall", *Geomech. Eng*., **17**(1), 109-118. http://doi.org/10.12989/gae.2019.17.1.109.

Vanneschi, C., Eyre, M., Burda, J., Zizka, L., Francioni, M. and Coggan, J.S. (2018), "Investigation of landslide failure mechanisms adjacent to lignite mining operations in North Bohemia (Czech Republic) through a limit equilibrium/finite element modelling approach", *Geomorphology*, **320**, 142-153. http://doi.org/10.1016/j.geomorph.2018.08.006.

Wang, L., Wu, C.Z., Li, Y.Q., Liu, H.L., Zhang, W.G. and Chen, X. (2019), "Probabilistic risk assessment of unsaturated slope failure considering spatial variability of hydraulic parameters", *KSCE J. Civ. Eng*., **23**(12), 5032-5040. http://doi.org/10.1007/s12205-019-0884-6.

Yamaguchi, K., Takeuchi, N. and Hamasaki, E. (2018), "Three-dimensional simplified slope stability analysis by hybrid-type penalty method", *Geomech. Eng*., **15**(4), 947-955. http://doi.org/10.12989/gae.2018.15.4.947.

Zhou, X.P., Cheng, H. and Wong, L.N.Y. (2019), "Three-dimensional stability analysis of seismically induced landslides using the displacement-based rigorous limit equilibrium method", *B. Eng. Geol. Environ*., **78**(7), 4743-4756. https://doi. org/10.1007/s10064-018-01444-4.

Zhu, D.Y., Lee, C.F., Qian, Q.H. and Chen, G.R. (2005). "A concise algorithm for computing the factor of safety using the Morgenstern-Price method", *Can. Geotech. J*., **42**(1), 272-278. https://doi.org/10.1139/t04-072.

GC